ADVANCED ELECTRONIC MATERIALS
www.advelectronicmat.de

Programmable Spin Logic Based on Spin Hall Effect in a Single Device

*Caihua Wan, Xuan Zhang, Zhonghui Yuan, Chi Fang, Wenjie Kong, Qintong Zhang, Hao Wu, Usman Khan, and Xiufeng Han**

Spin logic devices, due to their programmability and nonvolatility, are deemed as an ideal building block for the next generation of electronics. Though several types of spin logic based on domain wall motion, spin-field-effect transistor and automata made of magnetic nanoparticles have been proposed, an architecture with scalability, energy efficiency and compatibility with current complementary metal-oxide-semiconductor technology is still in urgent demand. Here, it is experimentally demonstrated that the spin Hall effect in magnetic films with perpendicular anisotropy can be utilized to construct such a spin logic device. Five commonly used logic gates with nonvolatility in a single device are realized. This demonstration could pave the way towards application of spintronics in logic circuits as well as the memory industry in the near future and could even give birth to logic-in-memory computing architectures.

1. Introduction

Due to nonvolatility, reconfigurability, and parallel computing capability, interest in magnetic logics,[1–14] especially a wide variety of novel spin logics,[1–8,12–14] is exponentially growing. Several spin logic schemes based on Oersted-field driven magnetic tunnel junction,[2] spin accumulation or current in semiconductors,[5,7,15] magnetic automata made of nanoparticles or nanochains,[1,4,8,13] magnetic domain walls motion,[3] spin torque oscillators,[16] and magnetoelectric effect[17] have been proposed. A few of them have even been experimentally demonstrated. However, the alternative techniques simultaneously containing programmability among the five commonly used logic gates, compatibility with current complementary metal-oxide-semiconductor (CMOS) technology, high operation speed, and good scalability are still lacking. Herein, we utilize spin Hall effect (SHE), which can convert charge current to pure spin current in high efficiency[18–22] and even switch the magnetization of thin films,[23–28] to construct programmable spin logic devices. In our design, five typically used Boolean logic gates of AND, OR, NOT, NOR, and NAND are simultaneously integrated into a single perpendicularly magnetized trilayer structure of Pt/Co/MgO stack in which an applied magnetic field serves as a switch among the different logic operations. This experimental demonstration provides a practical prototype of highly integrated multifunctional spin logic device that might be used as an elementary building block for future reconfigurable logic processor with high parallel computing speed, high densities, and compatibility with current magnetic random access memory (MRAM) and CMOS techniques.

Dr. C. H. Wan, X. Zhang, Dr. Z. H. Yuan, C. Fang, W. J. Kong, Dr. Q. T. Zhang, H. Wu, Dr. U. Khan, Prof, X. F. Han
Institute of Physics, University of Chinese Academy of Sciences
Chinese Academy of Sciences
Beijing National Laboratory for Condensed Matter Physics
Beijing 100190, China
E-mail: xfhan@iphy.ac.cn

DOI: 10.1002/aelm.201600282

2. Results and Discussions

Pt/Co/MgO and Ta/CoFeB/MgO perpendicular systems have been used due to their strong perpendicular magnetic anisotropy, large spin Hall angle, and high conversion efficiency from charge current to spin current as well as wide use in current MRAM technologies. In the following, only data from Pt/Co/MgO are presented here.

2.1. Magnetic Properties

As-deposited Pt(5)/Co(0.8)/MgO(2)/Pt(3 nm) stacks have in-plane anisotropy while they gradually exhibit perpendicular magnetic anisotropy (PMA) after annealing at and above 250 °C under perpendicular field of 7 kOe (**Figure 1**). Increase in annealing temperature significantly results in the decrease of coercivity while saturation field in hard axis (5 kOe) varies little above 300 °C. We have utilized the stack annealed at 400 °C to construct spin logic devices due to its robust PMA as well as small coercivity. The stacks are then patterned as Hall bar (Figure 1a) in which dimensions of magnetic films are 20 μm × 20 μm. Then a current of 1 mA in Pt leads to current density of 1 MA cm^{-2} in it. Dependences of Hall resistance (R_{xy}) of a typical Hall bar on magnetic field along the x, y, and z axes

 © 2017 WILEY-VCH Verlag GmbH & Co. KGaA, Weinheim

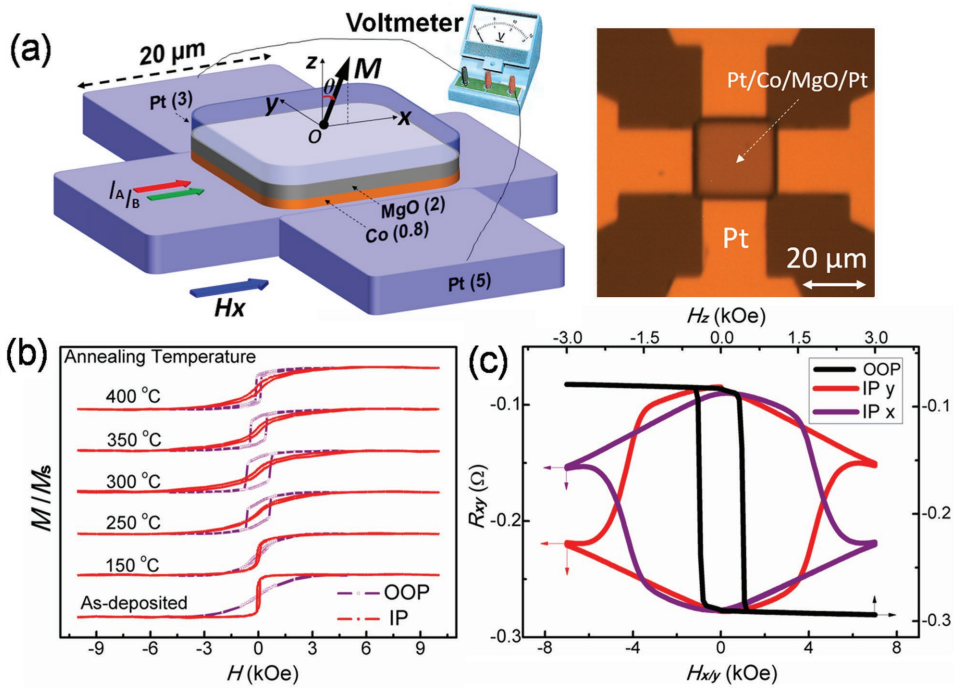

Figure 1. a) Patterned Hall bar geometry of a Pt/Co/MgO/Pt film with thin film dimensions of 20 μm × 20 μm. Unit of the numbers in parentheses is nanometer. A photo image of a real device is also shown. b) *M*–*H* curves of the same Pt/Co/MgO/Pt film as a function of annealing temperatures. c) Field dependences of R_{xy} of a Hall bar with field along the *x*, *y*, and *z* axes.

are shown in Figure 1c. Different from unpatterned films, the Hall bar shows larger coercivity and saturation field of 0.34 and 13.6 kOe, respectively, due to size reduction.

2.2. Current Switching Properties

As we apply both a current (I) and a magnetic field along the x axis (H_x), magnetization of the perpendicular Co can be switched due to SHE and as-induced spin–orbit torque (**Figure 2**), similar with the previous result.[25] We have applied two methods to characterize this switching process. In Method I (Figure 2a,c), large current pulses with 50 ms duration time are applied to control magnetization. Hall voltage is picked up at the end of each pulse. In this case volatile and nonvolatile deviations in magnetization induced by the large current pulse are simultaneously probed. In Method II (Figure 2b,d), large current pulses are first applied and after an interval time of 100 ms, we apply subsequently another very small current pulse (1 mA, 50 ms) at the end of which Hall voltage is picked up. In the second method, only nonvolatile change of magnetization induced by the first large current pulse is captured. Except better squareness and larger critical switching current in Method II, dependences of R_{xy} on applied current measured in the two methods share similar symmetries (panels (c) and (d)). Positive and negative current larger than a threshold switching current (I_C) supports spin-up and spin-down state, respectively, under positive H_x. Here I_C is defined as the current where $R_{xy}(I_C) = (R_{xy}^{\max} + R_{xy}^{\min})/2$ with $R_{xy}^{\max/\min}$ being the maximum/minimum value in the R_{xy} versus I curves. As the polarity of H_x is reversed, switching direction is also reversed. The I_C varies little as $|H_x|$ smaller than 1 kOe. In the following, only the results measured in Method II are presented. Switching behavior at larger H_x is similar to that at smaller H_x (Figure 2e). Especially, opposite H_x leads to opposite switching direction. However, a remarkable reduction of I_C is observed as $|H_x|$ between 1 and 3.5 kOe. The I_C decreases gradually from 76 mA at 0.5 kOe to 60 mA at 3.5 kOe (Figure 2f). The observed typical switching behavior can be well reproduced by a macrospin model after spin–orbit torque induced by spin Hall effect is taken into account (Section SI1, Supporting Information).

The dependence of magnetization (or Hall resistance) on applied current exhibits well defined threshold behavior, which endows us with an opportunity to construct a spin logic device based on threshold logic theory that mimics the working mechanism of human neurons.[29,30] Especially, the threshold current I_C could be tuned by a large amount via magnetic field, further promising the spin logic device versatile reconfigurability. In the following, tunability of I_C and reversibility of switching direction under opposite H_x are utilized to construct the spin logic device which is nonvolatile and programmable among five different gates.

2.3. Programmable Logic Operations

Data are stored in magnetization of Co film, spin-up state ($+m_z$) for 1 and spin-down state ($-m_z$) for 0. Stored data in magnetization can be retrieved via a magnetic tunnel junction (MTJ) in future application while they are read out here

© 2017 WILEY-VCH Verlag GmbH & Co. KGaA, Weinheim

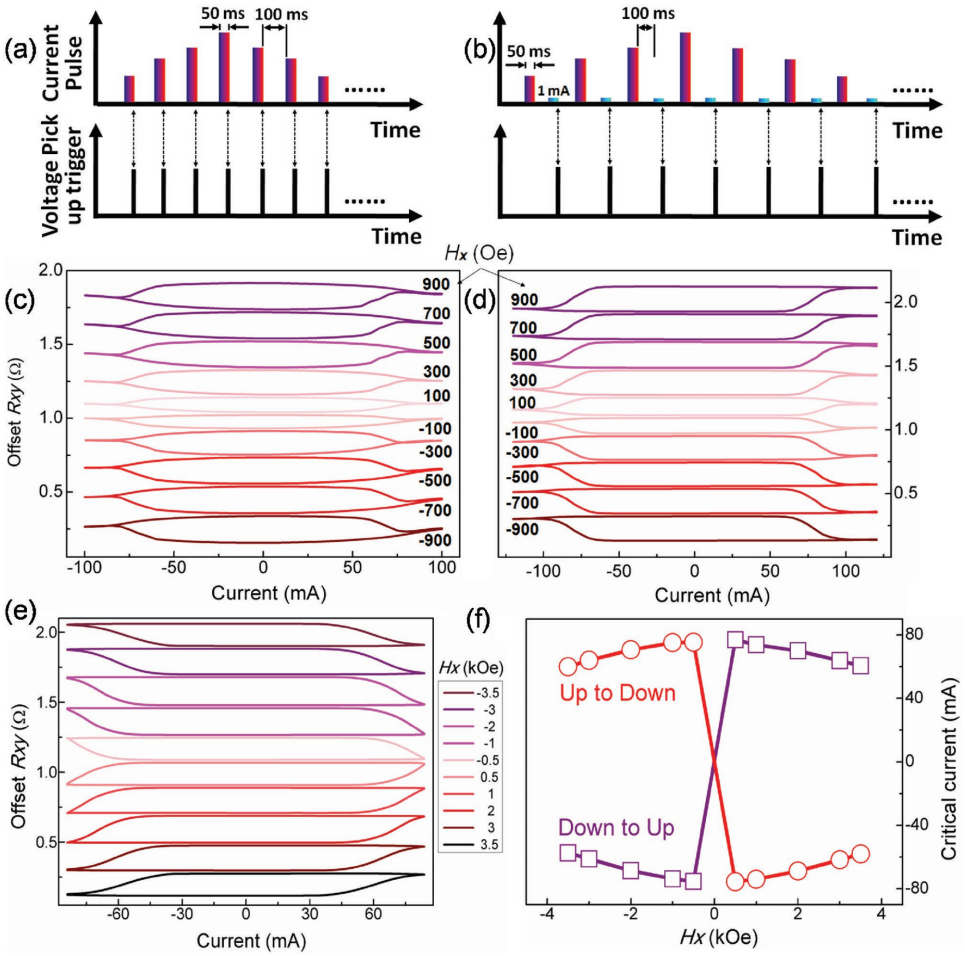

Figure 2. a,b) Two methods to measure dependence of R_{xy} on applied current (along x axis) under different magnetic fields H_x. c,d) R_{xy} versus I curves measured with (a) Method I and (b) Method II with $|H_x| < 1$ kOe. Method II only detects nonvolatile change of R_{xy} induced by large current pulses and a small pulse current of 1 mA is used to pick up R_{xy}. e) R_{xy} versus I under large H_x. f) I_C as a function of H_x for up-to-down transition (circles) and down-to-up transition (squares).

via R_{xy} for convenience. R_{xy} of 200 mΩ is set in the device (Section SI2, Supporting Information) as a benchmark above and below which m_z is identified as spin-up state ($+m_z$, logic 1) and spin-down state ($-m_z$, logic 0), respectively. Two currents I_A and I_B, functioning as two inputs, are applied both along the x axis. I_A and I_B are 42 and 24 mA for Inputs 1 and 0, respectively. H_x with magnitudes of ±0.5 and ±3.5 kOe is used to program this device among different logic gates. It is worth recalling that I_C values at 0.5 and 3.5 kOe are 76 and 60 mA, respectively (Figure 2f). The final magnetization state of Co film is thus determined by the value of $(I_A + I_B - I_C)$ as well as polarity of H_x. Similar with a proposed programmable logic gate based on magnetic tunnel junction driven by Oersted field,[2] our device also needs an initialization step and a subsequent operation step to perform the complete logic operation.

Figure 3 demonstrates that five logic gates (AND, OR, NOT, NOR, and NAND) have been all realized in a single device under different H_x. Truth tables of the five gates are shown in Figure 3a. For an "AND" gate (Figure 3b), H_x = 0.5 kOe is applied with threshold current I_C of 76 mA. Before logic operations, the device is initialized to $-m_z$ by $I_A = I_B = -42$ mA. If either input A or B is 0, $I_A + I_B < I_C$, which means the device retains its initial state $-m_z$ with Output 0. Only as A = B = 1 and $I_A + I_B > I_C$ can the device be switched to $+m_z$ (Output 1).

For an "OR" gate (Figure 3c), H_x is tuned to 3.5 kOe and I_C = 60 mA. The device is also initialized to $-m_z$ by $I_A = I_B = -42$ mA. Except A = B = 0, other input combinations all make $I_A + I_B > I_C$, leading to deterministic switching from $-m_z$ to $+m_z$.

For a "NOR" gate (Figure 3f), H_x = –3.5 kOe and I_C = 60 mA. Here switching direction is opposite to the case as H_x = 3.5 kOe. We still use $I_A = I_B = -42$ mA to initialize device, however, to $+m_z$. Only as A = B = 0 can the device retain its initial state $+m_z$. Or else the device is switched to $-m_z$ as either A or B is 1 or both of them are 1.

For a "NAND" gate (Figure 3e), H_x = –0.5 kOe, I_C = 76 mA. Initialization to $+m_z$ is also performed by $I_A = I_B = -42$ mA. In this case, only as A = B = 1 can the device be switched back to $-m_z$. Otherwise, the initial $+m_z$ state is retained.

For a "NOT" gate (Figure 3d), H_x = –0.5 kOe and I_C = 76 mA. In contrast to the other logic gates, here, only A is used as an

© 2017 WILEY-VCH Verlag GmbH & Co. KGaA, Weinheim

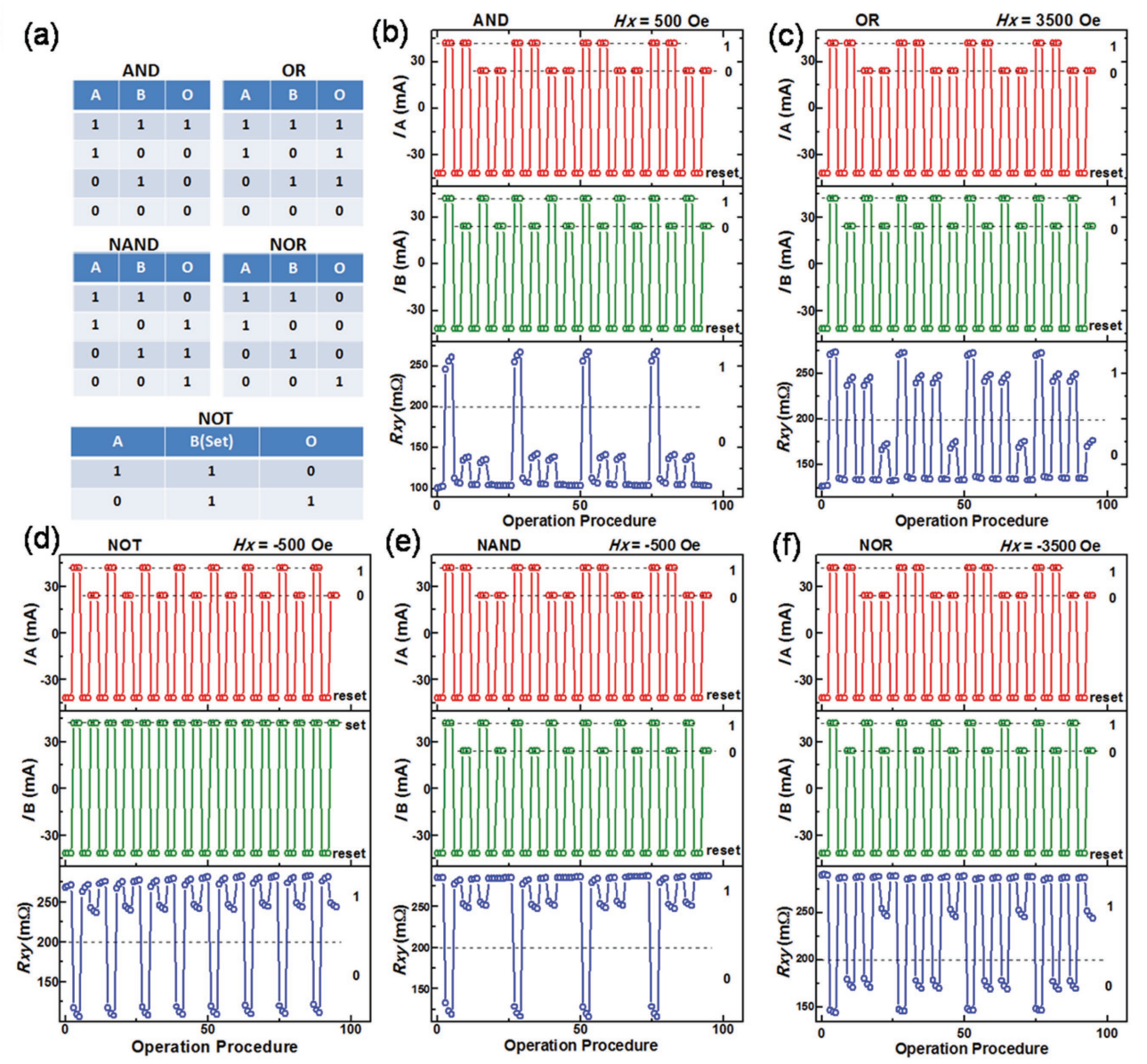

Figure 3. Logic operations of the spin logic device. a) Truth tables of the five gates. Input current I_A (upper), I_B (middle), and output R_{xy} (bottom) of a device in b) "AND," c) "OR," d) "NOT," e) "NAND," and f) "NOR" gate, respectively. Inputs 1 and 0 are 42 and 24 mA, respectively. Before each logic operation, −42 mA of I_A and I_B are simultaneously applied to reset device to a proper initial state. Each operation was conducted three times to show reproducibility. Only 4 periods of each logic gate are shown to demonstrate reproducibility though more than 4 periods have been conducted.

input while B just assists in initializing device as well as writing output. We first apply $I_A = I_B = -42$ mA to initialize the device to $+m_z$. Keeping $I_B = 42$ mA stable, we can set the device to $-m_z$ or keep the device in the original $+m_z$ state via Input A = 1 or 0, respectively. We have also measured other two Pt/Co/MgO/Pt devices. They exhibit the similar characteristics. Spin logic devices made of Ta/CoFeB/MgO/Pt stacks have also been experimentally realized. Besides, calculated logic operation based on the macrospin model is attached in Section SI3 (Supporting Information). The simulated results well reproduce characteristics of Figure 3.

2.4. A Way toward Practical Spin Logic Devices

Besides of a complete set of Boolean operations and nonlinear transport characteristics, a practical logic device should also have strong enough output to drive another device.[7] Moreover, according to requirement of feedback prevention, output of a device should not influence its own input.[7] Therefore, three-terminal MTJ[23] with the perpendicular Pt/Co/MgO or Ta/CoFeB/MgO film as a free layer could be ideally utilized to construct such a practical spin logic device. In this kind of device, input currents are applied only through the heavy metal while output

© 2017 WILEY-VCH Verlag GmbH & Co. KGaA, Weinheim

current is applied through the MTJ, automatically satisfying feedback prevention requirement. Furthermore, a device could output a large or small current according to its magnetization state, parallel or antiparallel state, respectively. And the large or small current could be further introduced into the heavy metal of the next logic device as Input 1 or 0, respectively. In this way cascading is realized. Zhang et al. has already proved feasibility of this cascading manner in simulations.[31] Here we just used the Pt/Co/MgO and Ta/CoFeB/MgO (free layer of a practical three-terminal MTJ device) to demonstrate the complete set of Boolean operations, which is the most important requirement for a logic device. Furthermore, spin–orbit torque induced magnetization switching can be achieved within 0.1–1 ns,[32,33] physically promising this device fast operating speed. Nonvolatility of magnetization state further endows the device unprecedented capability of parallel computing as elaborated in details by Ney[2] and Sidhu,[34] which could further increase computing efficiency compared with conventional serial architecture. Though dimension of the demo devices is 20 μm here, there is no physical limit to prevent three-terminal MTJ devices scaling down to 100 nm or below,[35,36] which could greatly increase the density and reduce power of a real spin logic chip based on the working mechanism proposed in this research.

3. Conclusion

In summary, five logic gates (AND, OR, NOT, NOR, and NAND) in a single device are experimentally demonstrated via spin Hall effect. Programmability of the device is encoded in tunability of I_C and reversibility of switching direction under different H_x. Our work not only experimentally manifests that spin logic building block integrable with current MRAM and CMOS technologies could be conveniently realized by spin Hall effect in the perpendicular system, but also sheds light on a feasible pathway toward a nonvolatile, programmable, and highly parallel logic-in-memory architecture in the near future.

4. Experimental Section

Pt(5)/Co(0.8)/MgO(2)/Pt(3) and Ta(5)/$Co_{20}Fe_{60}B_{20}$(1)/MgO(2)/Pt(3) (thickness in nanometer) stacks were magnetron-sputtered at room temperature. They bear intrinsically in-plane anisotropy. Only after high-temperature annealing above 150 °C in a normal field of 0.7 T did the stacks begin to exhibit strong perpendicular anisotropy (Figure 1b,c). Raw films were then patterned by ultraviolet lithography and the following two-step argon ion etching into Hall bars with the size of the center squares being 20 μm (Figure 1a). Cu(10 nm)/Au(30 nm) electrodes were finally deposited to make contacts with four legs of Hall bars. After device microfabrication, the Hall bars were measured by normal 4-terminal methods with Keithley 2400 and Keithley 2182 sourcing devices and measuring Hall voltages, respectively. Meanwhile, PPMS-9T (Quantum Design) provided magnetic fields with proper directions. For logic operations and magnetization switching measurements, two different measurement procedures were adopted. In Method I, a Keithley 2400 first provided a large current pulse to Hall bar for 50 ms to destabilize magnetization and then Keithley 2182 picked up Hall voltage at the end of each pulse. In Method II, the Keithley 2400 first provided large current pulse to the Hall bar. Then it was switched off after the pulse. After 100 ms wait, another small current of 1 mA was provided to the Hall bar. Keithley 2182 then measured Hall voltage at the end of the small current pulse. After another 100 ms, the next round of destabilizing-measuring process was performed. During logic operations, two Keithley 2400 sources provide I_A and I_B at the same time to destabilize magnetization.

Supporting Information

Supporting Information is available from the Wiley Online Library or from the author.

Acknowledgements

C.H.W. and X.Z. contributed equally to this work. This research was supported by the MOST National Key Scientific Instrument and Equipment Development Projects [No. 2011YQ120053], the 863 Plan Project of Ministry of Science and Technology (MOST) (Grant No. 2014AA032904), National Natural Science Foundation of China [NSFC, Grant Nos. 11434014, 51229101, and 11404382], and the Strategic Priority Research Program (B) of the Chinese Academy of Sciences (CAS) [Grant No. XDB07030200]. Perpendicular Pt/Co/MgO and Ta/CoFeB/MgO stacks were provided by Singulus Technologies AG, Germany.

Received: July 19, 2016
Revised: December 14, 2016
Published online:

[1] R. P. Cowburn, M. E. Welland, *Science* **2000**, *287*, 1466.
[2] A. Ney, C. Pampuch, R. Koch, K. H. Ploog, *Nature* **2003**, *425*, 485.
[3] D. A. Allwood, G. Xiong, C. C. Faulkner, D. Atkinson, D. Petit, R. P. Cowburn, *Science* **2005**, *309*, 1688.
[4] A. Imre, G. Csaba, L. Ji, A. Orlov, G. H. Bernstein, W. Porod, *Science* **2006**, *311*, 205.
[5] H. Dery, P. Dalal, L. Cywinski, L. J. Sham, *Nature* **2007**, *447*, 573.
[6] X. Han, Z. Wen, Y. Wang, L. Wang, H. Wei, *AAPPS Bull.* **2008**, *18*, 25.
[7] B. Behin-Aein, D. Datta, S. Salahuddin, S. Datta, *Nat. Nanotechnol.* **2010**, *5*, 266.
[8] A. A. Khajetoorians, J. Wiebe, B. Chilian, R. Wiesendanger, *Science* **2011**, *332*, 1062.
[9] S. Joo, T. Kim, S. H. Shin, J. Y. Lim, J. Hong, J. D. Song, J. Chang, H. W. Lee, K. Rhie, S. H. Han, K. H. Shin, M. Johnson, *Nature* **2013**, *494*, 72.
[10] Z. Luo, C. Xiong, X. Zhang, Z. Guo, J. Cai, X. Zhang, *Adv. Mater.* **2016**, *28*, 2760.
[11] Z. Luo, X. Zhang, C. Xiong, J. Chen, *Adv. Funct. Mater.* **2015**, *25*, 158.
[12] D. E. Nikonov, I. A. Young, *Proc. IEEE* **2013**, *101*, 2498.
[13] D. Bhowmik, L. You, S. Salahuddin, *Nat. Nanotechnol.* **2014**, *9*, 59.
[14] S. Manipatruni, D. E. Nikonov, I. A. Young, *Phys. Rev. Appl.* **2016**, *5*, 014002.
[15] S. Datta, B. Das, *Appl. Phys. Lett.* **1990**, *56*, 665.
[16] I. Krivorotov, D. Markovic, presented at *MIND Annual Review and NRI Benchmarking Workshop*, Notre Dame, IN August **2011**.
[17] D. E. Nikonov, I. A. Young, *J. Mater. Res.* **2014**, *29*, 2109.
[18] J. Sinova, S. O. Valenzuela, J. Wunderlich, C. H. Back, T. Jungwirth, *Rev. Mod. Phys.* **2015**, *87*, 1213.
[19] A. Hoffmann, *IEEE Trans. Magn.* **2013**, *49*, 5172.
[20] J. E. Hirsch, *Phys. Rev. Lett.* **1999**, *83*, 1834.
[21] S. Zhang, *Phys. Rev. Lett.* **2000**, *85*, 393.
[22] T. Kimura, Y. Otani, T. Sato, S. Takahashi, S. Maekawa, *Phys. Rev. Lett.* **2007**, *98*, 156601.

 © 2017 WILEY-VCH Verlag GmbH & Co. KGaA, Weinheim

[23] L. Liu, C. F. Pai, Y. Li, H. W. Tseng, D. C. Ralph, R. A. Buhrman, *Science* **2012**, *336*, 555.
[24] M. I. Miron, K. Garello, G. Gaudin, P. J. Zermatten, M. V. Costache, S. Auffret, S. Bandiera, B. Rodmacq, A. Schuhl, P. Gambardella, *Nature* **2011**, *476*, 189.
[25] L. Liu, O. J. Lee, T. J. Gudmundsen, D. C. Ralph, R. A. Buhrman, *Phys. Rev. Lett.* **2012**, *109*, 096602.
[26] A. van den Brink, G. Vermijs, A. Solignac, J. Koo, J. T. Kohlhepp, H. J. M. Swagten, B. Koopmans, *Nat. Commun.* **2016**, *7*, 10854.
[27] S. Fukami, C. Zhang, S. D. Gupta, A. Kurenkov, H. Ohno, *Nat. Mater.* **2016**, *15*, 535.
[28] X. Zhang, C. H. Wan, Z. H. Yuan, Q. T. Zhang, H. Wu, L. Huang, W. J. Kong, C. Fang, U. Khan, X. F. Han, *Phys. Rev. B* **2016**, *94*, 174434.
[29] R. Rojas, *Neural Networks: A Systematic Introduction*, Springer, Berlin **1996**.
[30] D. Hampel, R. O. Winder, *IEEE Spectrum* **1971**, *8*, 32.
[31] Y. Zhang, B. Yan, W. Wu, H. Li, Y. Chen, *Proc. of the 2015 Design, Automation & Test in Europe Conference & Exhibition (DATE)* Grenoble, France **2015**, pp. 1000–1005.
[32] K. Garello, C. O. Avci, I. M. Miron, M. Baumgartner, A. Ghosh, S. Auffret, O. Boulle, G. Gaudin, P. Gambardella, *Appl. Phys. Lett.* **2014**, *105*, 212402.
[33] M. Sasikanth, E. N. Dmitri, A. Y. Ian, *Appl. Phys. Express* **2014**, *7*, 103001.
[34] R. P. S. Sidhu, A. Mei, V. K. Prasanna, in *Field-Programmable Logic and Applications* (Eds: P. Lysaght, J. Irvine, R. W. Hartenstein), Springer, Berlin **1999**.
[35] X. F. Han, Z. C. Wen, H. X. Wei, *J. Appl. Phys.* **2008**, *103*, 07E933.
[36] S. Ikeda, K. Miura, H. Yamamoto, K. Mizunuma, H. D. Gan, M. Endo, S. Kanai, J. Hayakawa, F. Matsukura, H. Ohno, *Nat. Mater.* **2010**, *9*, 721.

© 2017 WILEY-VCH Verlag GmbH & Co. KGaA, Weinheim